The British Journal of Radiology, 83 (2010), 241–251

Schedule for CT image guidance in treating prostate cancer with helical tomotherapy

[1]G BELDJOUDI, [1,2]S YARTSEV, PhD, [1,2]G BAUMAN, MD, FRCPC, [1,2]J BATTISTA, PhD and [1,2]J VAN DYK, MSc

[1]*London Regional Cancer Program, London Health Sciences Centre, and* [2]*The University of Western Ontario, London, Ontario N6A 4L6, Canada*

ABSTRACT. The aim of this study was to determine the effect of reducing the number of image guidance sessions and patient-specific target margins on the dose distribution in the treatment of prostate cancer with helical tomotherapy. 20 patients with prostate cancer who were treated with helical tomotherapy using daily megavoltage CT (MVCT) imaging before treatment served as the study population. The average geometric shifts applied for set-up corrections, as a result of co-registration of MVCT and planning kilovoltage CT studies over an increasing number of image guidance sessions, were determined. Simulation of the consequences of various imaging scenarios on the dose distribution was performed for two patients with different patterns of interfraction changes in anatomy. Our analysis of the daily set-up correction shifts for 20 prostate cancer patients suggests that the use of four fractions would result in a population average shift that was within 1 mm of the average obtained from the data accumulated over all daily MVCT sessions. Simulation of a scenario in which imaging sessions are performed at a reduced frequency and the planning target volume margin is adapted provided significantly better sparing of organs at risk, with acceptable reproducibility of dose delivery to the clinical target volume. Our results indicate that four MVCT sessions on helical tomotherapy are sufficient to provide information for the creation of personalised target margins and the establishment of the new reference position that accounts for the systematic error. This simplified approach reduces overall treatment session time and decreases the imaging dose to the patient.

Received 28 October 2008
Revised 9 April 2009
Accepted 29 April 2009

DOI: 10.1259/bjr/28706108

Image guidance for daily localisation is becoming increasingly used in conjunction with advanced delivery techniques such as intensity-modulated radiation therapy [1–11]. Pre-treatment imaging facilitates dose escalation and organ at risk (OAR) sparing through a reduction in the planning target volume (PTV) margin customised to account for daily variation in patient anatomy and set-up [12–30]. Helical tomotherapy (HT) is an image guidance delivery platform combining on-board megavoltage CT (MVCT) imaging and intensity-modulated irradiation [31–34]. MVCT acquisition is used routinely at our centre for daily image registration with the reference kilovoltage CT (kVCT) for adjustment of patient positioning prior to treatment. However, the MVCT imaging, registration and patient repositioning steps represent approximately 40% of the overall treatment session time [35]. Therefore, optimisation of the image localisation procedure is important for improved (cost–benefit aspect) utilisation of the unit [36–38]. In addition to positioning correction, the acquisition of daily imaging also provides new opportunities for dose adaptive radiotherapy (ART) [39, 40]. With the HT platform, Planned Adaptive® software (TomoTherapy Inc. Madison, WI) is available that allows the delivered dose distribution to be calculated using the MVCT study and fluence sinograms of the same day. Adjustments of structure contours can be included to reflect daily anatomy changes and to study the impact of subsequent adaptation of the plan. Adaptive planning applied either retrospectively or prospectively using daily CT imaging provides unique opportunities for delivery verification and adaptive re-planning, respectively [41, 42]. Simulation of various dose delivery options allows for assessment of the effects on the dose distribution of set-up misalignment or internal anatomy changes. Furthermore, adaptive planning, when used in conjunction with dose distribution recalculation, allows prospective plan modification if a deformation or tumour regression is considered clinically unacceptable. Recently, the Orlando group reported an interesting retrospective study of the residual localisation errors with different imaging scenarios [43, 44], but they did not explore the impact of different imaging options on the accumulated dose delivery, as done in this work.

In this study, we used the daily set-up correction shifts for 20 prostate cancer patients to explore opportunities for safe reduction of the number of imaging procedures. The goal was to find the minimal number of MVCT sessions that allows for correction of the systematic error in positioning specific to the patient. Information about the random error obtained during these sessions allows personalised PTV margins to be created for the remaining

Address correspondence to: Slav Yartsev, Department of Physics and Engineering, LRCP/LHSC, 790 Commissioners Road East, London, Ontario N6A 4L6, Canada. E-mail: slav.yartsev@lhsc.on.ca

treatment fractions. The Planned Adaptive® software is used for evaluation of the dose distribution with a reduced number of imaging sessions. Optimal schedules for imaging and/or plan adaptation for prostate cancer cases are discussed.

Methods and patients

Patient population

In the current Hi-ART® version (TomoTherapy Inc. Madison, WI) of HT, the same linear accelerator is used both for radiation treatment with 6 MV X-rays and for MVCT imaging with 3.5 MV X-rays [34]. A mutual information algorithm is used for co-registration of kVCT and MVCT studies to detect daily position corrections and visualise anatomy variations. The co-registration images can be viewed in transverse, coronal and sagittal cross-sections, and manual adjustments are applied, if necessary. Since clinical use of HT commenced in our institution (September 2004), daily MVCT studies have always preceded each radiation treatment, and the geometric shifts made after the co-registration step for each fraction of treatment have been recorded. The results for the first 20 patients treated for prostate cancer were reviewed for this study, incorporating a total of 700 MVCT images. For all of the patients, the clinical target volume (CTV) covered at minimum the whole prostate gland and the PTV was expanded from the CTV by adding an isotropic 10 mm margin.

Set-up corrections

In a recent paper, we analysed the average of the shifts in the lateral $\bar{x}_k$, superior–inferior $\bar{y}_k$ and anteroposterior $\bar{z}_k$ directions over k fractions (k = 1,2,3,…, n, where n is the total number of fractions) [45]. The average of patient shifts over all n fractions $(\bar{x}_n, \bar{y}_n, \bar{z}_n)$ would give the most accurate average shift based on repeated daily imaging. Based on the full set of acquired data for the 20 patients treated, we simulated what deviations may be expected in the case of a reduced number of imaging sessions ($k<n$):

$$\begin{cases} \delta_x(k) = \bar{x}_k - \bar{x}_n, \\ \delta_y(k) = \bar{y}_k - \bar{y}_n, \\ \delta_z(k) = \bar{z}_k - \bar{z}_n. \end{cases} \quad (1)$$

To choose the ''optimal'' number of imaging sessions, denoted ''i'' in what follows, we analyse the values of $\delta(k)$ as a function of k for different directions (x, y, z) and for different patients. When the average of $\delta(k)$ over all patients is below a given level of acceptability or threshold level, this number of imaging sessions is considered as optimal number i. Such a threshold level can be set by comparing with the uncertainty of 3 mm in prostate delineation by physicians on MVCT studies during the co-registration step [46].

We define the interfraction motion tendency $\bar{\Psi}(i)$ by using information from only the first i set-up shifts:

$$\bar{\Psi}(i) = \begin{cases} \bar{\Psi}_x(i) = \frac{1}{i}\sum_{m=1}^{i} |x_m - \bar{x}_i| \\ \bar{\Psi}_y(i) = \frac{1}{i}\sum_{m=1}^{i} |y_m - \bar{y}_i| \\ \bar{\Psi}_z(i) = \frac{1}{i}\sum_{m=1}^{i} |z_m - \bar{z}_i| \end{cases} \quad (2)$$

This represents the average residual localisation error when using the imaged fractions with a correction based on the average shift over i fractions (these values will be used as a modified set-up position $(\bar{x}_i^0, \bar{y}_i^0, \bar{z}_i^0)$ for the remaining fractions without imaging). The parameters $\bar{\Psi}_x(i)$, $\bar{\Psi}_y(i)$, $\bar{\Psi}_z(i)$ contain patient-specific information about the trends in interfraction motion and can be used to calculate the margin (in most cases anisotropic) around the CTV to create a ''personalised'' PTV for the rest of the treatment.

The database of shifts made at the co-registration step was used to evaluate what would be the residual error using the actual shifts based on the daily MVCT studies for treatment fractions (i+1) to n with respect to the modified set-up position $(\bar{x}_i^0, \bar{y}_i^0, \bar{z}_i^0)$ calculated using the MVCT studies of the first i fractions. The absolute value of the vector shift

$$R(i,m) = \sqrt{(x_m - \bar{x}_i^0)^2 + (y_m - \bar{y}_i^0)^2 + (z_m - \bar{z}_i^0)^2}, \quad m = (i+1),(i+2),\ldots,n \quad (3)$$

provides three-dimensional information on the actual shift for fraction m, based on the MVCT study of this day relative to the modified set-up position $(\bar{x}_i^0, \bar{y}_i^0, \bar{z}_i^0)$.

The averages over all fractions m from i+1 to n of the actual shifts with respect to the modified set-up position $(\bar{x}_i^0, \bar{y}_i^0, \bar{z}_i^0)$ are:

$$\bar{R} = \begin{cases} \bar{R}_x(i) = \frac{1}{n-i}\sum_{m=i+1}^{n} \left|x_m - \bar{x}_i^0\right| \\ \bar{R}_y(i) = \frac{1}{n-i}\sum_{m=i+1}^{n} \left|y_m - \bar{y}_i^0\right| \\ \bar{R}_z(i) = \frac{1}{n-i}\sum_{m=i+1}^{n} \left|z_m - \bar{z}_i^0\right| \end{cases} \quad 1 \le i \le n-1 \quad (4)$$

These parameters have been calculated for all patients included in this study.

In order to check the reliability of the prediction $\bar{\Psi}(k)$ for patient interfraction motion, we calculated the absolute values of difference ($\Delta(k)$) between predicted $\bar{\Psi}(k)$ (see Equation 2) and actual average shifts during fractions (k+1) to n, $\bar{R}(k)$, (see Equation 4) for each direction:

$$\Delta(k) = \begin{cases} \Delta_x(k) = \left|\bar{R}_x(k) - \bar{\Psi}_x(k)\right| \\ \Delta_y(k) = \left|\bar{R}_y(k) - \bar{\Psi}_y(k)\right| \\ \Delta_z(k) = \left|\bar{R}_z(k) - \bar{\Psi}_z(k)\right| \end{cases} \quad (5)$$

for k varying from 2 to 9 for the 20 patients. Analysis of these data may be used to choose the optimal number i of

imaging sessions when $\Delta(i)$, the ''error due to non-imaging during fractions from $(i+1)$ to n'', is below an acceptable threshold in all directions.

In this study, we had information about the target position in all n fractions for 20 patients and so could assess the inaccuracy of predicting interfraction motion using residual deviations in the limited number (k) of imaging sessions. We added the error margin given by the difference $\Delta(k)$ between residual shift data obtained during the first k fractions, $\bar{\Psi}(k)$, and the actual residual shifts, $\bar{R}(k)$, observed in the remaining fractions.

Simulation of delivered dose distribution

Simulation of different imaging scenarios and verification of the delivered dose were performed with the Planned Adaptive® (Tomotherapy Inc.) software. In the first option, the MVCT studies of any fraction k were placed, with respect to the planning kVCT study, in accordance with the shifts applied by the therapists on that day. The prostate volume and shape were assumed not to change during treatment [47]; thus, the same positioning shifts were applied to the CTV and PTV contours determined by co-registration of the MVCT studies. As the bladder and rectum volumes are subject to daily changes, the outlines of the rectum and the bladder were adapted by deformation of their contours on each slice of the MVCT for each fraction. The dose distribution calculated with the Planned Adaptive® software using the delivered fluence sinogram of the day, pre-treatment MVCT images and adapted contours is termed the ''daily verification dose''. Summing up the daily verification doses for all fractions resulted in an overall verification dose. In the second option, in order to simulate the consequences for the dose distribution of a reduced ($k=i$) imaging schedule, we summed up the parameters obtained from dose–volume histograms (DVHs) of the first i fractions, applying actual shifts and adjusting contours as in the first option but, for the days $k>i$, placing the daily MVCT image sets and the structure contours to the modified set-up position $(\bar{x}_i^0, \bar{y}_i^0, \bar{z}_i^0)$ representing the average shift during the first i fractions. In this manner, we simulated the consequences for the dose distribution of limiting the number of imaging sessions. For the analysis, a DVH for each fraction was obtained and the parameters of the dose distribution for each fraction were summed for the whole treatment course and compared with the planned goals.

In addition to providing set-up corrections, the information about patient set-up shifts obtained during first i imaging sessions could be useful ''to personalise'' the PTV margins for plan adaptation during the remaining treatment (without CT imaging) from fraction $(i+1)$ to fraction n. Indeed, if we assume that the patient would have the same trend to move in a particular direction for the non-imaged residual fractions as in the initial i fractions with MVCT imaging, we can adapt (increase or reduce) the PTV size anisotropically and thus preserve irradiation of the target with improved sparing of the OARs [48–51]. With our database of MVCT studies for patients with prostate cancer for all fractions, we evaluated this assumption by using Equations 1 and 3 for calculation of the average deviation from the actual shifts with respect to the $(\bar{x}_i^0, \bar{y}_i^0, \bar{z}_i^0)$ position in the x, y and z directions.

Currently, there are several methods to define the PTV margin; five of them were discussed by Hugo et al [51]. A working party of the British Institute of Radiology provided the general approach to estimating sizes of uncertainties and how to combine them in order to define the PTV [52]. Chapter 5 of its report gives a detailed description of systematic and treatment execution errors for calculation of PTV margins for the prostate. The group in William Beaumont Hospital proposed to construct a patient-specific PTV in the adaptive treatment process for prostate cancer [53]. We used the latter approach [51, 53] where the relation

$$\text{Total random error} = \sqrt{(\text{interfraction motion})^2 + (\text{intrafraction motion})^2} \quad (6)$$

is used to determine the global movement of the prostate by taking into account the inter- and intrafraction motion. Published data on the prostate intrafractional motion suggest that an additional internal margin of more than 2.5 mm may be needed to account for this motion [54–63], with reports of some cases where this motion is greater than 1 cm [64, 65]. For our study, the positional error owing to intrafraction motion was considered to be 4 mm [66, 67].

Results

Patients

Two particular patients have been selected for special attention in this group. Patient A, who was especially large (135 kg), was chosen for this study because of the large shifts observed during treatment: 9.8 ± 7.0 mm in the lateral (x-axis) direction, -1.7 ± 2.1 mm in the longitudinal (superior–inferior, y-axis) direction and 11.4 ± 3.1 mm in the vertical (anteroposterior, z-axis) direction with respect to the initial placement on external marks. Patient B was selected because of the largest average shift (by comparison with other patients) made in the z direction (17.0 ± 2.6 mm) and moderate shifts in other directions (1.6 ± 1.5 mm in x and -4.1 ± 1.2 mm in y directions). Table 1 presents physical parameters, as well as the prescription doses for these two ''special'' patients.

Optimal number of imaging sessions i

Daily shifts from MVCT/kVCT co-registration were analysed for all fractions for all 20 patients in this study. Some patients presented with significant variations in correction shifts for individual treatment fractions, as shown in Figure 1a for patient A. However, for most patients, the shifts in each direction were more stable, as was the case for patient B illustrated in Figure 1b.

Figure 2 illustrates the deviations $\delta(k)$ of average shifts calculated with a limited number of imaging sessions from the ''all fractions imaging'' option. The daily shift

Table 1. Patient characteristics and planning objectives

Patient	Age (years)	Weight (kg)	Height (cm)	Prescription in 35 fractions
A	69	135	163	73 Gy for 95% of the GTV (2.08 Gy/fraction) 70 Gy for 95% of the PTV_{70} (around the prostate) (2.00 Gy/fraction) 54 Gy for 95% of the PTV_{54} (around the seminal vesicles) (1.54 Gy/fraction)
B	75	102	167	73 Gy for 95% of the GTV and PTV (around the prostate) (2.08 Gy/fraction)

PTV, planning target volume; GTV, gross tumour volume.

data for 20 prostate cancer patients were used to calculate the population average of these deviations [45]. Our analysis in the case of only four fractions (k=4) with MVCT imaging is presented in Table 2 and shows that the population average of the deviation vector $\delta(4)$ is 1.53 mm. Using only four fractions, 16/20, 15/20 and 11/20 patients demonstrated a deviation $\delta(4)$ less than 1 mm in the x, y and z directions, respectively.

The $R(4,m)$ values (see Equation 1) for each patient have been calculated for the m fractions (m=5 to n) and are illustrated in Figure 3 for two of our patients. The average over m fractions of these vectors, $\bar{R}(4)$, has been calculated for each patient and plotted in Figure 4. The components of the residual error $\bar{R}(4)$ (see Equation 4) for our set of 20 patients are given in Table 2. The average of the vector shift around the position $(\bar{x}_4^0, \bar{y}_4^0, \bar{z}_4^0)$, $<\bar{R}(4)>$, over the population is 3.93 ± 1.29 mm; the maximum $\bar{R}(4)$ is obtained for Patient A and is equal to 8.22 mm.

A reasonable trade-off between improving accuracy and increasing workload points to the choice of the optimal number of fractions with MVCT as k=i=4, with the maximal deviations $\Delta(4)$ below 3 mm in all directions (see Table 2). In this case, parameters $\bar{\Psi}_x(4)$, $\bar{\Psi}_y(4)$ and $\bar{\Psi}_z(4)$ provide information about residual patient mobility in the x, y and z directions, respectively, once systematic error is accounted for by using the average reset position $(\bar{x}_4^0, \bar{y}_4^0, \bar{z}_4^0)$ obtained for the first four MVCT imaging sessions. The population average and maximum values for components of $\Delta(4)$ are presented in Table 2.

Anisotropic PTV design

For Patient A, $\bar{\Psi}_x(4)$=7.4 mm, $\bar{\Psi}_y(4)$=2.0 mm and $\bar{\Psi}_z(4)$=2.7 mm, so the interfraction motion uncertainty was estimated as 10.4 mm, 5.0 mm and 5.7 mm in the x, y and z directions, respectively. Using Equation 6 and an estimate of 4 mm for intrafraction target motion [61], the margin for the CTV to obtain the PTV was rounded up to 12 mm, 7 mm and 7 mm margins in x, y and z directions, respectively, for our calculations.

For Patient B, the interfraction motion tendency $\bar{\Psi}(4)$ was 3.6 mm in the x and y directions and 4.9 mm in the z direction. These values led to a three-dimensional anisotropic margins of 6 mm, 6 mm and 7 mm in the x, y and z direction, respectively. In order to test the sensitivity of the PTV margin on the method of their construction, we have investigated the option where, instead of deviation mean values (Equation 2), the standard deviations of the shifts (representing random error) with respect to the average are used for estimations of the interfraction motion; very similar values for the PTV margins were found.

Verification dose

For Patients A and B, new PTVs with anisotropic margin values were created on the planning kVCT studies, and new dose distributions were computed on the tomotherapy planning station. Figure 6 shows initial and adapted contours for the PTV of Patient B, and the DVHs for plans with isotropic and adapted ''personalised'' PTVs are presented in Figure 7 for this patient. The delivery sinograms of both initial and adapted plans were used to simulate the treatment with the adjusted PTVs. In the case of Patients A and B, the results for selected parameters of the dose distribution calculated for initial plan are shown in the columns denoted ''10 mm 3D PTV margin'' in Table 3. Contours for the

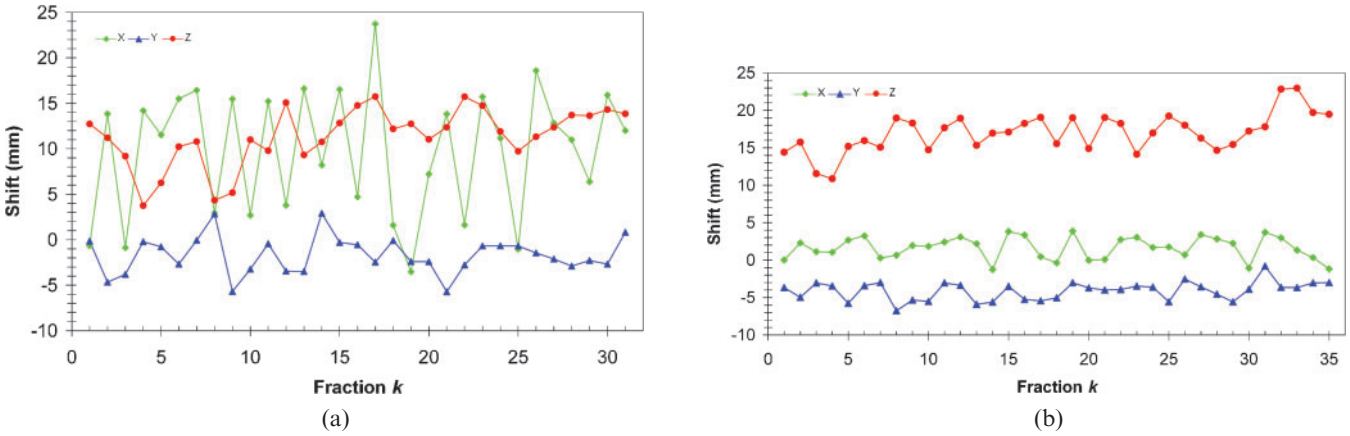

Figure 1. Set-up shifts obtained after matching megavoltage CT and kilovoltage CT studies on different days for Patients A (a) and B (b) in three directions.

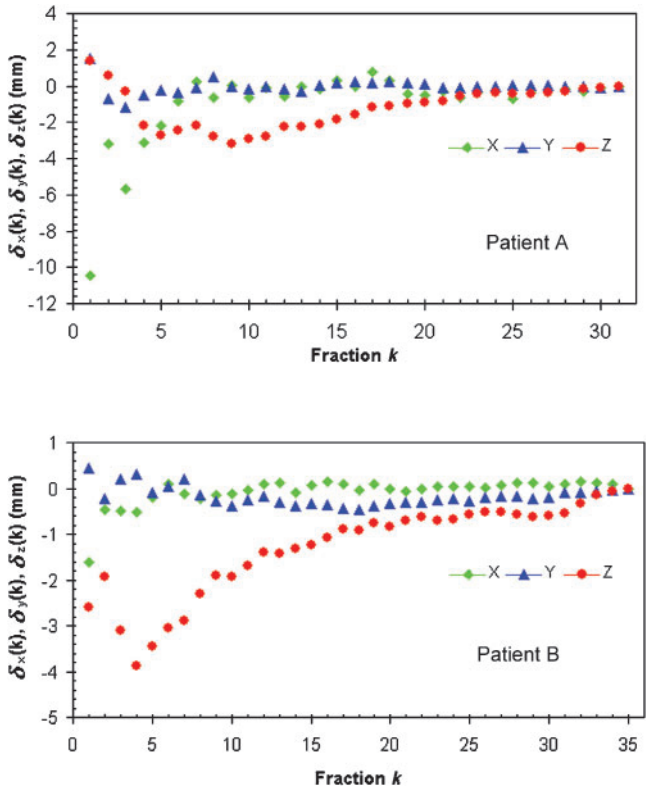

Figure 2. Examples for two patients of deviation $\delta(k)$. These represent the average shift over k fractions minus the average shift over all n fractions, for different directions.

bladder and rectum were adjusted of each daily MVCT, resulting in similar average bladder (144 cm^3 and 146 cm^3) and rectum (49 cm^3 and 48 cm^3) volumes for Patients A and B, respectively.

For patient A, the minimum dose to the CTV in the simulation scenario with $i=4$ is only 0.7 Gy less than the planned value and is still clinically acceptable. The rectum receives a lower dose than planned owing to predominant shifts in the lateral direction and the contour adaptation. The bladder $D_{15\%}$ dose is higher by 3.2 Gy than in the case of daily imaging but is still below the threshold fixed by the Radiation Therapy Oncology Group (RTOG) (bladder $D_{15\%}=80$ Gy).

For Patient B, the CTV irradiation in the case of imaging for the four first fractions is almost the same as that planned. In the new plan, the bladder receives a higher dose (but still below the RTOG constraint) and the rectum has better sparing.

For the 20 prostate cancer patients in this study, the point dose metrics have been found to be very close (within $\pm 2\%$) to the values obtained in the initial plans, proving the efficiency of image guidance with daily MVCT.

Discussion

The choice of the number of imaging sessions $i=4$ appears to be a good trade-off between MVCT workload and the value of the average residual error $\delta(4)$ after using a standardised shift (modified set-up position) based on a reduced number of MVCT images over the 20 patients, which is significantly less than 2 mm in all three directions (see Table 2). A 2 mm value appears acceptable if compared with the error of 3 mm in the prostate detection by the physician on the MVCT studies during the co-registration step [46]. Amer et al [29] and de Boer and Heijmen [30] have found that three imaging days provide an effective off-line correction of systematic positional errors. For image guidance with cone-beam CT, Nairz et al [6] analysed the data from six initial imaging sessions and concluded that the gain of accuracy was the largest during the first three sessions. Bortfeld et al [68] determined that four is the optimal number for measuring set-up errors by minimising the expectation value of the total quadratic set-up error taken over all fractions. Hoogeman et al [49] also favoured four imaging sessions.

To determine the significance of the PTV adaptation, a simulated dose distribution was re-calculated with Planned Adaptive® software. There are several approaches to PTV margin construction [14, 19, 27, 48, 51–54, 65, 69]. We have no intention of entering into a debate over which approach to the PTV margin creation is preferred. The stress is on the ability to diminish the number of imaging sessions and the ability of Planned Adaptive® software to check the dosimetric consequence of such a limitation. The choice of the way in which to create the PTV margin is defined by the accepted clinical practice in each institution. We have chosen the margins based on Equation 6 to take into account both intrafraction motion and patient-specific

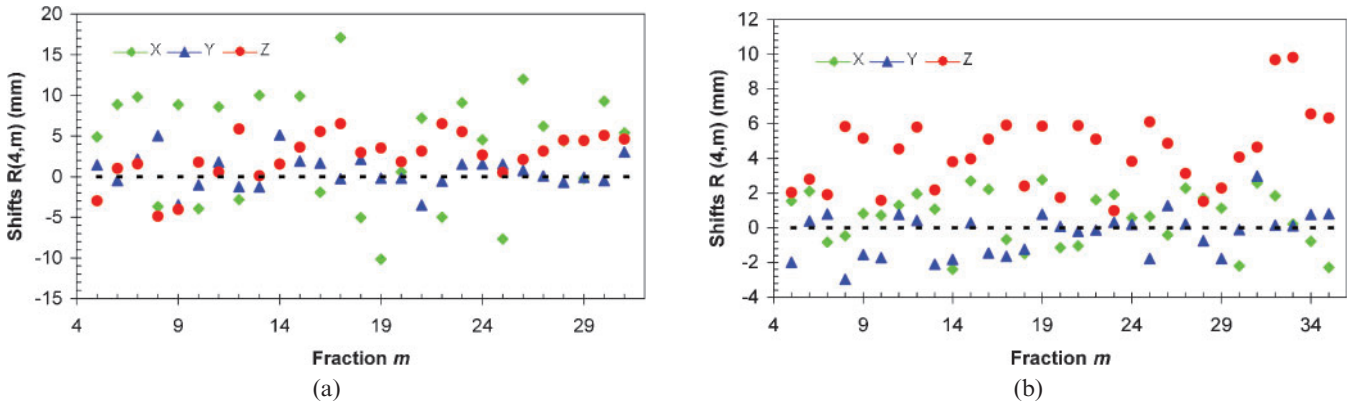

Figure 3. Set-up shifts with respect to the modified reference position $(\bar{x}_4^0, \bar{y}_4^0, \bar{z}_4^0)$ defined as the average shift over the first four fractions for Patients A (a) and B (b).

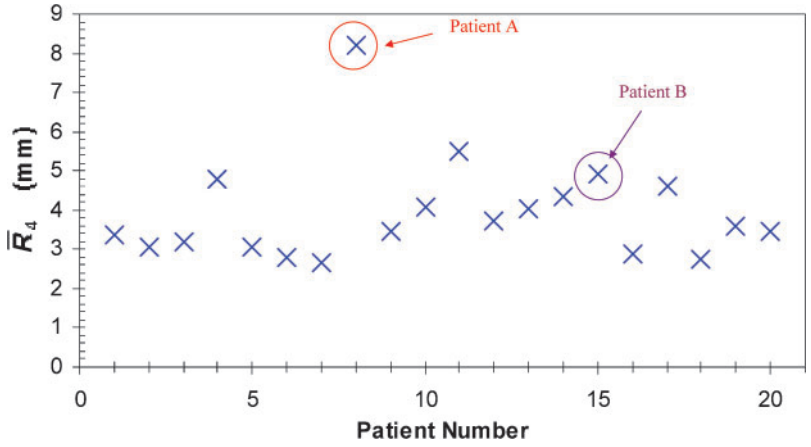

Figure 4. Average over fractions 5 to *n* of the three-dimensional displacements $\bar{R}(4)$ with respect to the modified reference position $(\bar{x}_4^0, \bar{y}_4^0, \bar{z}_4^0)$ for 20 prostate cancer patients.

information about his/her tendency for interfraction motion given by Equation 2. The effect of the use of personalised PTV margins is presented in Table 3 for Patients A and B, with a comparison to the case of an isotropic 10 mm PTV margin. For Patient A, comparing the plans made with an anisotropic (specific for this patient) margin and a three-dimensional isotropic 10 mm margin shows that the use of an adapted PTV allows better sparing for both the bladder and the rectum. The table also presents the parameters obtained by simulating the case with daily imaging for the first four fractions, patient repositioning to $(\bar{x}_4^0, \bar{y}_4^0, \bar{z}_4^0)$, and treatment without MVCT scanning for the remaining fractions. The adapted PTV shows a slight decrease in CTV coverage by only 0.9 Gy compared with what would be achieved with daily imaging (comparison between columns seven and six in Table 3). Owing to an interfraction motion tendency to shift this patient in the negative z direction, the rectum receives more dose (but still within the RTOG constraints) and the bladder is better spared.

For Patient B, the comparison made between columns 7 and 6 (Table 3) shows good coverage of the CTV (difference of 0.2 Gy with the plan) and less dose to both the rectum and the bladder by using an adapted PTV. As discussed by Yan et al [53], a PTV adapted for the majority of the treatment fraction may be used either for dose escalation to the target with rectum isotoxicity or for improved sparing of OARs.

Different parameters were evaluated for each of the simulation scenarios, with i ranging from 1 to 9, and compared with what was initially planned and accepted clinically. The following parameters were evaluated: $D_{99\%}$ for the CTV; $D_{99\%}$ for the PTV; D_{7cc}, D_{30cc} and $D_{15\%}$ for the bladder; and $D_{15\%}$ and D_{15cc} for the rectum. We

Table 2. Population averages and maximum values for different quantities introduced in Equations 1, 4 and 5 to measure the uncertainties introduced by a reduced number of imaging sessions

Direction	δ(4) (mm)	Max δ(4) (mm)	R(4) (mm)	Max R(4) (mm)	Δ(4) (mm)	Max Δ(4) (mm)
x	0.89±0.93	3.15	2.05±1.34	6.62	0.85±0.82	2.15
y	0.65±0.47	1.83	1.63±0.44	2.77	0.65±0.484	2.09
z	1.12±0.86	3.87	2.11±0.78	4.37	0.83±0.61	2.44

Table 3. Dose–volume histogram parameters (Gy) for treatments with daily imaging and for a simulated option with imaging for four fractions followed by the patient positioned on $(\bar{x}_4^0, \bar{y}_4^0, \bar{z}_4^0)$ for fractions 5 to *n*. A comparison of cases with isotropic 10 mm and adapted (anisotropic) PTV margins

Patient	Structure	Parameter	10 mm 3D PTV margins		Adapted 3D PTV margins	
			Planning dose	Simulation dose	Planning dose	Simulation dose
A	GTV	$D_{99\%}$	72.2	71.5	72.0	71.1
	PTV_{70}	$D_{99\%}$	69.5	57.9	69.1	58.1
	Bladder	$D_{15\%}$	61.5	64.7	58.5	60.6
		D_{7cc}	72.1	72.1	69.4	66.8
		D_{30cc}	63.7	51.2	59.5	58.1
	Rectum	$D_{15\%}$	68.5	66.7	62.6	63.4
		D_{15cc}	60.3	59.0	56.9	56.9
B	GTV	$D_{99\%}$	74.0	73.97	72.8	72.6
	PTV	$D_{99\%}$	69.4	62.2	71.1	58.4
	Bladder	$D_{15\%}$	72.3	74.1	66.1	70.2
		D_{7cc}	74.5	75.5	73.7	74.8
		D_{30cc}	68.3	71.4	61.4	65.6
	Rectum	$D_{15\%}$	70.3	64.9	64.9	60.8
		D_{15cc}	52.3	52.1	50.6	50.9

PTV, planning target volume; 3D, three-dimensional; GTV, gross tumour volume.

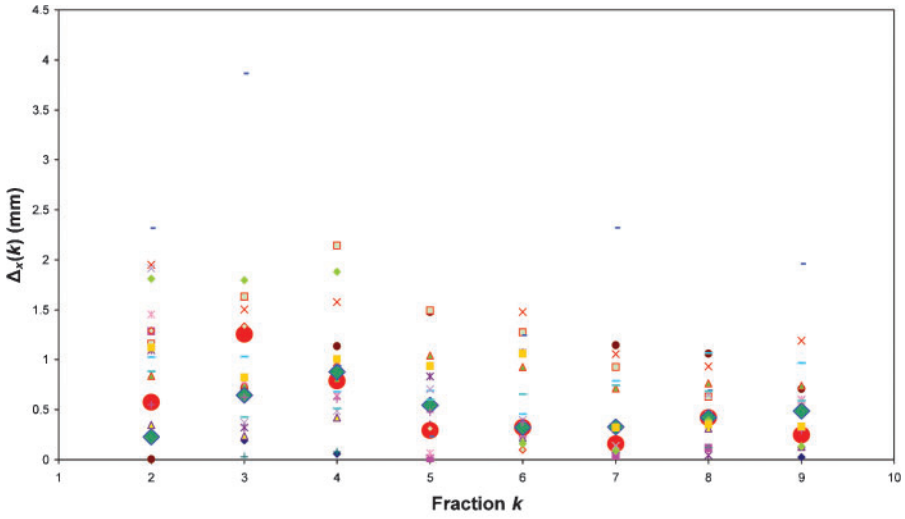

(a)

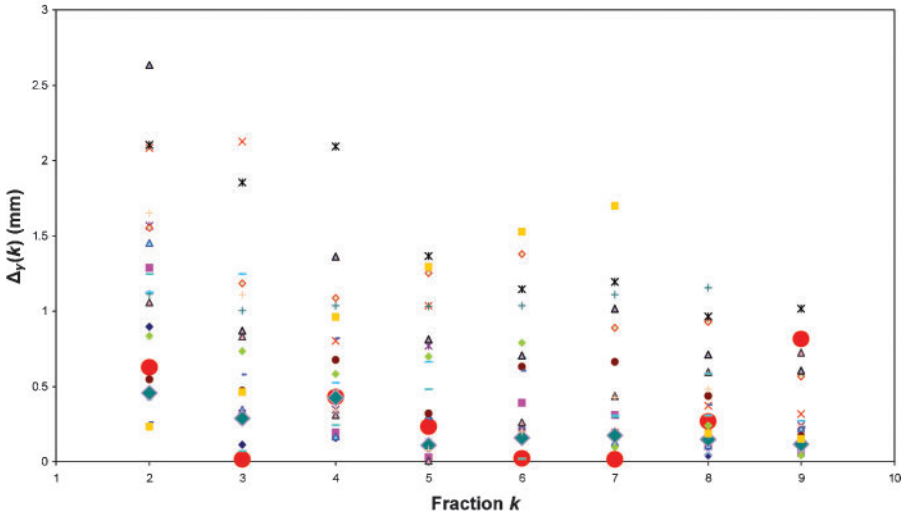

(b)

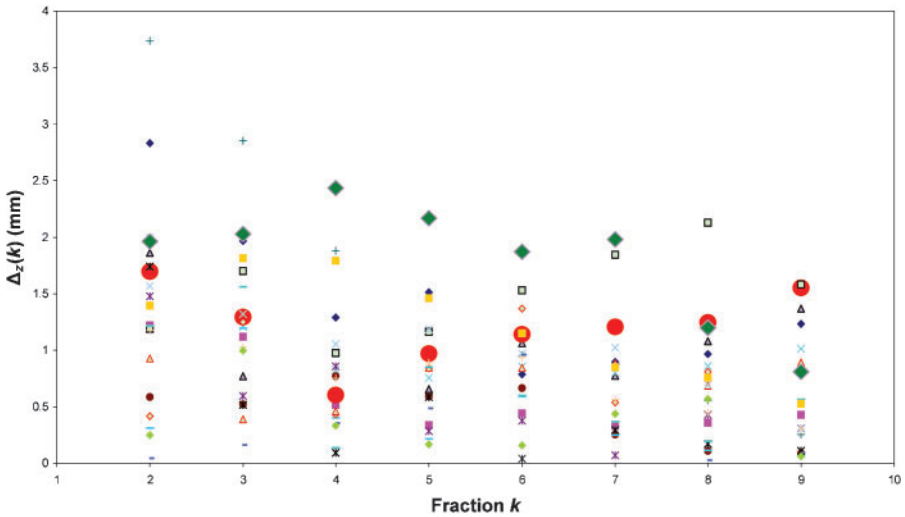

(c)

Figure 5. Absolute values of the difference $\Delta(k)$ between predicted average shifts, $\bar{\Psi}(k)$, and observed average shifts, $\bar{R}(k)$, for (a) *x*, (b) *y* and (c) *z* directions. Data are for the 20 patients included in this study. Large circles denote data for Patient A and large diamonds data for Patient B.

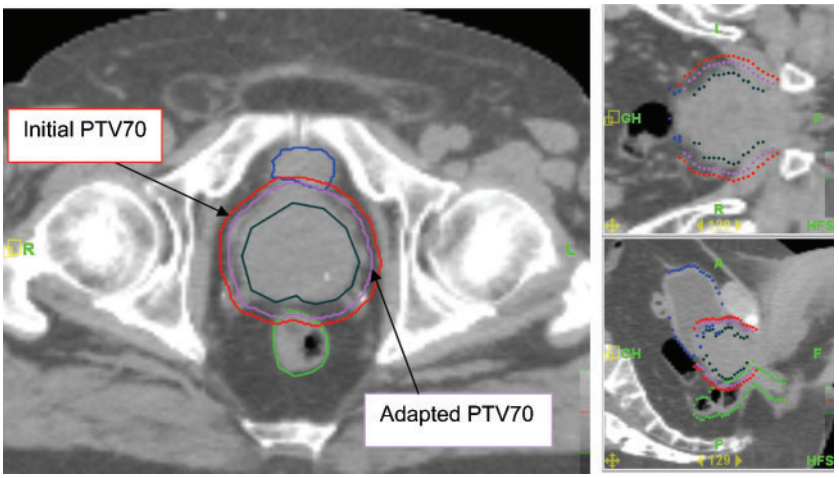

Figure 6. The initial planning target volume (PTV) with isotropic 10 mm margins (red lines) and adapted PTV with personalised anisotropic margins (turquoise lines) for Patient B.

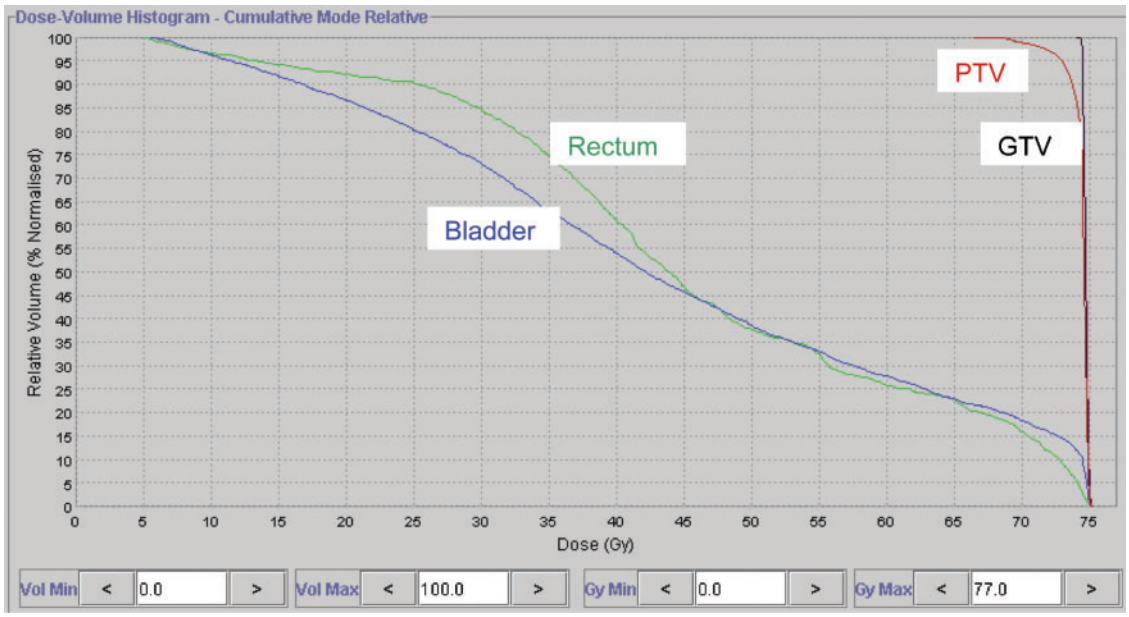

(a)

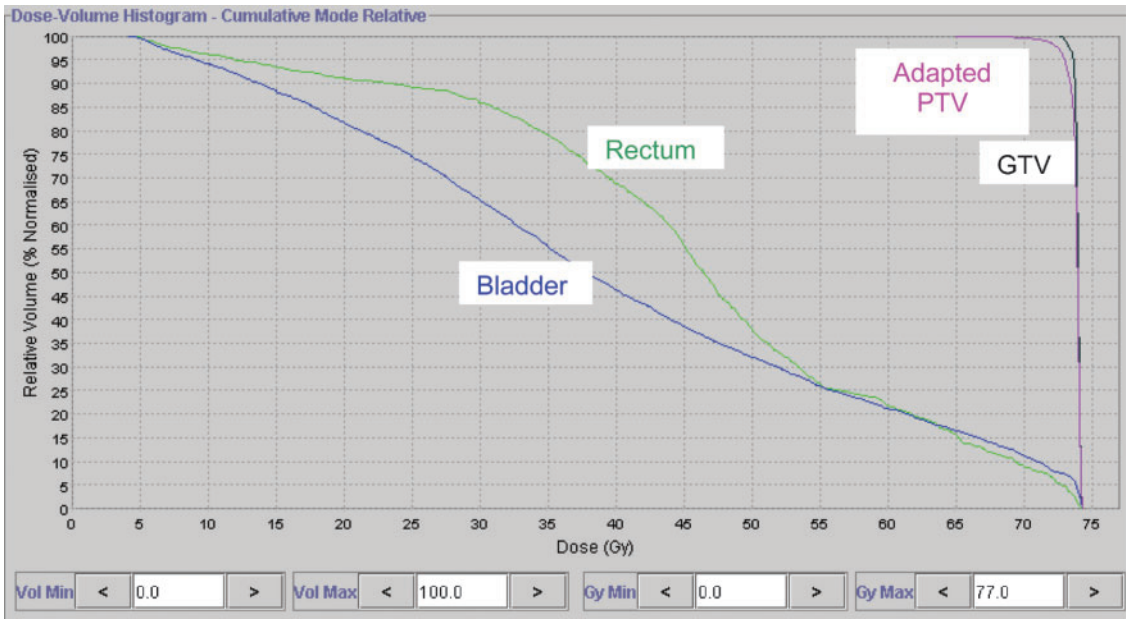

(b)

Figure 7. Comparison of dose–volume histograms in (a) initial and (b) adapted plans for Patient B.

note that, owing to daily changes of the prostate and rectum volumes, the parameter $D_{15\%}$ is less informative than the absolute fixed volumes D_{7cc} and D_{30cc} for the bladder and D_{15cc} for the rectum. The clinical significance of D_{7cc} and D_{30cc} for the bladder was discussed by Harsolia et al [70], whereas the significance of D_{15cc} for the rectum was proposed by Kupelian et al [71] as an indicator of rectal bleeding. We should note that the daily verification dose calculated with Planned Adaptive® does not take into account the effect of organ deformation [72]; therefore, point dose metrics for the overall verification dose (D_{max}, D_{min}, D_{5cc}, etc.) may not be accurate when summed in this fashion. This is likely to be more of an issue for bladder and rectum volumes than for the prostate, which is stable in volume.

The question of imaging dose is currently under active discussion [73, 74]. In our practice, each MVCT delivers ~1.2 cGy per acquisition (with daily imaging of 42 cGy or <0.6% of prescription), which is less than MV portal images and of the same order as the dose from cone beam CT [74]. Our evaluation of the optimal number of imaging sessions offers a compromise between delivery precision and shortened in-room time and lower total imaging dose to the patient.

In the future it would be interesting to explore a correlation between a patient's specific features and the interfraction prostate motion. Indeed, if some physical particularities could be identified (weight, prostate size, prostate shape, etc.) as a predictive factor of the patient's future interfraction motion, some groups of patients could be identified *a priori* in order to adapt different imaging protocols specific to each cohort. Patient A, for example, was the heaviest patient of the group of 20 and was suffering from rectal bleeding and strong pain in the legs owing to arthritis. These few elements could explain why this patient had such irregularities in his positioning on the couch. Studies on a larger patient database would be beneficial (especially to answer the question of adequate threshold value for registration shift correction), and more simulated dose distribution calculations for various imaging scenarios need to be done before optimal imaging and treatment options for a particular patient can be determined.

Conclusions

We have shown that only four sessions of MVCT imaging on a tomotherapy unit are normally sufficient to account for the systematic set-up error, with clinically acceptable accuracy for prostate radiotherapy. Moreover, the daily shifts in three directions registered during these first four fractions allow us to determine the general tendency of a patient to move in a particular direction and thus permit the characterisation of the interfraction motion specific to this patient. Based on these characteristics of the interfraction motion, new ''personalised'' PTV margins can be created to assure the improved irradiation of the CTV and/or sparing of the organs at risks. The use of the Planned Adaptive® software allowed the evaluation of the effects of daily MVCT imaging *vs* scenarios of the limited number of imaging sessions and adaptation of the PTV margin.

Acknowledgments

This study was conducted with the support of the Ontario Institute for Cancer Research through funding provided by the government of Ontario.

References

1. Verellen D, De Ridder M, Storme G. A (short) history of image-guided radiotherapy. Radiother Oncol 2008;86:4–13.
2. Dawson LA, Jaffray DA. Advances in image-guided radiation therapy. J Clin Oncol 2007;25:938–46.
3. White E, Kane G. Radiation medicine practice in the image-guided radiation therapy era: new roles and new opportunities. Semin Radiat Oncol 2007;17:298–305.
4. Xing L, Thorndyke B, Schreibmann E, Yang Y, Li TF, Kim GY, et al. Overview of image guided radiation therapy. Med Dosim 2006;31:91–112.
5. Ippolito E, Mertens I, Haustermans K, Gambacorta MA, Pasini D, Valentini V. IGRT in rectal cancer. Acta Oncol 2008;47:1317–24.
6. Nairz O, Merz F, Deutschmann H, Kopp P, Schöller H, Zehentmayr F. A strategy for the use of image-guided radiotherapy (IGRT) on linear accelerators and its impact on treatment margins for prostate cancer patients. Strahlenther Onkol 2008;184:663–7.
7. Redpath AT, Wright P, Muren LP. The contribution of on-line correction for rotational organ motion in image-guided radiotherapy of the bladder and prostate. Acta Oncol 2008;47:1367–72.
8. O'Neill L, Armstrong J, Buckney S, Assiri M, Cannon M, Holmberg O. A phase II trial for the optimisation of treatment position in the radiation therapy of prostate cancer. Radiother Oncol. 2008;88:61–6.
9. Li HS, Chetty IJ, Enke CA, Foster RD, Willoughby TR, Kupellian PA, et al. Dosimetric consequences of intrafraction prostate motion. Int J Radiat Oncol Biol Phys 2008;71:801–12.
10. McGrath S, Kestin L, Dilworth J, Liang J, Krauss D, Yan D, et al. Adaptive image guided radiotherapy (IGRT) eliminates the risk of geometric miss due to rectal distention in prostate cancer treatment planning: biochemical and clinical evidence of efficacy [Abstract]. Int J Radiat Oncol Biol Phys 2008;72:S324.
11. Wang W, Wu Q, Yan D. Quantitative evaluation of cone beam computed tomography in target volume definition for offline image guided radiation therapy of prostate cancer (Abstract). Int J Radiat Oncol Biol Phys 2008;72:S550–1.
12. Grills, IS, Hugo G, Kestin LL, Galerani AP, Chao KK, Wloch J, et al. Image-guided radiotherapy via daily online cone-beam CT substantially reduces margin requirements for stereotactic lung radiotherapy. Int Radiat Oncol Biol Phys 2008;70:1045–56.
13. Moseley DJ, White EA, Wiltshire KR, Rosewall T, Sharpe MB, Siewerdsen JH, et al. Comparison of localization performance with implanted fiducial markers and cone-beam computed tomography for on-line image-guided radiotherapy of the prostate. Int J Radiat Oncol Biol Phys 2007;67:942–53.
14. Poulsen PR, Muren LP, Høyer M. Residual set-up errors and margins in on-line image-guided prostate localization in radiotherapy. Radiother Oncol 2007;85:201–6.
15. Soete G, Verellen D, Michielsen D, Vinh-Hung V, Van de Steene J, Van den Berge D, et al. Clinical use stereoscopic X-ray positioning of patients treated with conformal radiotherapy for prostate cancer. Int J Radiat Oncol Biol Phys 2002;54:948–52.
16. Sorcini B, Tilikidis A. Clinical application of image-guided radiotherapy, IGRT (on the Varian OBI platform). Cancer Radiother 2006;10:252–7.

17. Kerkhof EM, Put RW, Raaymakers BW, van der Heide UA, van Vulpen M, Lagendijk JJ. Variation in target and rectum dose due to prostate deformation: an assessment by repeated MR imaging and treatment planning. Phys Med Biol 2008;53:5623–34.
18. Goulet CC, Herman MG, Hillman DW, Davis BJ. Estimated limits of IMRT dose escalation using varied planning target volume margins. Phys Med Biol 2008;53:3777–88.
19. Meijer GJ, de Klerk J, Bzdusek K, van den Berg HA, Janssen R, Kaus MR, et al. What CTV-to-PTV margins should be applied for prostate irradiation? Four-dimensional quantitative assessment using model-based deformable image registration techniques. Int J Radiat Oncol Biol Phys 2008;72:1416–25.
20. Hammoud R, Patel SH, Pradhan D, Kim J, Guan H, Li S, et al. Examining margin reduction and its impact on dose distribution for prostate cancer patients undergoing daily cone-beam computed tomography. Int J Radiat Oncol Biol Phys 2008;71:265–73.
21. Gordon JJ, Siebers JV. Evaluation of dosimetric margins in prostate IMRT treatment plans. Med Phys 2008;35:569–75.
22. Huang SH, Catton C, Jezioranski J, Bayley A, Rose S, Rosewall T. The effect of changing technique, dose, and PTV margin on therapeutic ratio during prostate radiotherapy. Int J Radiat Oncol Biol Phys 2008;71:1057–64.
23. Zhang M, Moiseenko V, Liu M. PTV margin for dose escalated radiation therapy of prostate cancer with daily online realignment using internal fiducial markers: Monte Carlo approach and dose population histogram (DPH) analysis. J Appl Clin Med Phys 2006;7:38–49.
24. Gordon JJ, Siebers JV. Convolution method and CTV-to-PTV margins for finite fractions and small systematic errors. Phys Med Biol 2007;52:1967–90.
25. Gordon JJ, Crimaldi AJ, Hagan M, Moore J, Siebers JV. Evaluation of clinical margins via simulation of patient setup errors in prostate IMRT treatment plans. Med Phys 2007;34:202–14.
26. Poli ME, Parker W, Patrocinio H, Souhami L, Shenouda G, Campos LL, et al. An assessment of PTV margin definitions for patients undergoing conformal 3D external beam radiation therapy for prostate cancer based on an analysis of 10,327 pretreatment daily ultrasound localizations. Int J Radiat Oncol Biol Phys 2007;67:1430–7.
27. van Herk M, Remeijer P, Rasch C, Lebesque JV. The probability of correct target dosage: Dose–population histograms for deriving treatment margins in radiotherapy. Int J Radiat Oncol Biol Phys 2000;47:1121–35.
28. Craig T, Satkusagingham J, Chan K, Brock K, Moseley J, Chung P, et al. Advanced image guidance allows margin reduction in radiation therapy of prostate cancer [Abstract]. Int J Radiat Oncol Biol Phys 2008;72:S551.
29. Amer AM, Mackay RI, Roberts SA, Hendry JH, Williams PC. The required number of treatment imaging days for an effective off-line correction of systematic errors in conformal radiotherapy of prostate cancer. Radiother Oncol 2001;61:143–50.
30. de Boer HCJ, Heijmen BJM. A protocol for the reduction of systematic patient setup errors with minimal portal imaging workload. Int J Radiat Oncol Biol Phys 2001;50:1350–65.
31. Mackie TR, Balog J, Ruchala K, Shepard D, Aldridge S, Fitchard E, et al. Tomotherapy. Sem Radiat Oncol 1999;9:108–17.
32. Mackie TR. History of tomotherapy. Phys Med Biol 2006;51:R427–53.
33. Welsh JS, Patel RR, Ritter MA, Harari PM, Mackie TR, Mehta MP. Helical tomotherapy: an innovative technology and approach to radiation therapy. Technol Canc Res Treat 2002;1:311–6.
34. Ruchala KJ, Olivera GH, Schloesser EA, Mackie TR. Megavoltage CT on a tomotherapy system. Phys Med Biol 1999;44:2597–621.
35. Tomsej M. The TomoTherapy Hi Art System® for sophisticated IMRT and IGRT with helical delivery: recent developments and clinical applications. Cancer Radiother 2006;10:288–95.
36. Maggiulli E, Broggi S, Pierelli A, Cattaneo G, Canandrino R. 2007 Validation of KVCT-MVCT automatic registration techniques on a helical tomotherapy unit (HT) and estimation of the capabiliuty to point out set-up errors. Proc ICCR 2007;2:180–4.
37. Woodford C, Yartsev S, Van Dyk J. Optimization of megavoltage CT scan registration settings for brain cancer treatments on tomotherapy. Phys Med Biol 2007;52: N185–93.
38. Woodford C, Yartsev S, Van Dyk J. Optimization of megavoltage CT scan registration settings for thoracic cases on helical tomotherapy. Phys Med Biol 2007;52:N345–54.
39. Ramsey CR, Langen KM, Kupelian PA, Scaperoth DD, Meeks SL, Mahan SL, et al. A technique for adaptive image-guided helical tomotherapy for lung cancer. Int J Radiat Oncol Biol Phys 2006;64:1237–44.
40. Welsh JS, Lock M, Harary P, Tomé W. Clinical implementation of adaptive helical tomotherapy: A unique approach to image-guided intensity modulated radiotherapy. Technol Canc Res Treat 2006;5:465–80.
41. Kupelian PA, Willoughby TR, Reddy CA, Klein EA, Manadevan A. Impact of image guidance on outcome after external beam radiotherapy for localized prostate cancer. Int J Radiat Oncol Biol Phys 2008;70:1146–50.
42. Nijkamp J, Pos FJ, Nuver TT, de Jong R, Remeijer P, Sonke JJ, et al. Adaptive radiotherapy for prostate cancer using kilovoltage cone-beam computed tomography: first clinical results. Int J Radiat Oncol Biol Phys 2008;70:75–82.
43. Meeks S, Kupelian PA, Lee C, Willoughby T, Zeidan O, Langen K. Does image guidance need to be performed daily in the treatment of localized prostate cancers? Implications on treatment margins [Abstract]. Int J Radiat Oncol Biol Phys 2007;69:S82–3.
44. Kupelian PA, Lee C, Langen KM, Zeidan OA, Mañon RR, Willoughby TR, et al. Evaluation of image-guidance strategies in the treatment of localized prostate cancer. Int J Radiat Oncol Biol Phys 2008;70:1151–7.
45. Beldjoudi G, Yartsev S, Battista JJ, Van Dyk J. Optimisation of MVCT imaging schedule in prostate cancer treatment using helical tomotherapy. Cancer Radiother. 2008;12: 316–22.
46. Song WY, Chiu B, Bauman GS, Lock M, Rodrigues G, Ash R, et al. Prostate contouring uncertainty in megavoltage computed tomography images acquired with a helical tomotherapy unit during image-guided radiation therapy. Int J Radiat Oncol Biol Phys 2006;65:595–607.
47. Deurloo KE, Steenbakkers RJ, Zijp LJ, de Bois JA, Nowak PJ, Rasch CR, et al. Quantification of shape variation of prostate and seminal vesicles during external beam radiotherapy. Int Radiat Oncol Biol Phys 2005;61:228–38.
48. Beltran C, Herman MG, Davis BJ. Planning target margin calculations for prostate radiotherapy based on intrafraction and interfraction motion using four localization methods. Int J Radiat Oncol Biol Phys 2008;70:289–95.
49. Hoogeman MS, van Herk M, de Bois J, Lebesque JV. Strategies to reduce the systematic error due to tumor and rectum motion in radiotherapy of prostate cancer. Radiother Oncol 2005;74:177–85.
50. Vargas C, Yan D, Kestin LL, Krauss D, Lockman DM, Brabbins DS, et al. Phase II dose escalation study of image-guided adaptive radiotherapy for prostate cancer: Use of dose–volume constraints to achieve rectal isotoxicity. Int J Radiat Oncol Biol Phys 2005;63:141–9.

51. Hugo GD, Yan D, Liang J. Population and patient specific target margins for 4D adaptive radiotherapy to account for intra- and inter-fraction variation in lung tumour position. Phys Med Biol 2007;52:257–74.
52. Bidmead M, Coffey M, Crellin A, Dobbs J, Driver D, Greener T, et al (editors). Geometric uncertainties in radiotherapy: defining the planning target volume. London, UK: British Institute of Radiology, 2003.
53. Yan D, Lockman D, Brabbins D, Tyburski L, Martinez A. An off-line strategy for constructing a patient specific planning target volume in adaptive treatment process for prostate cancer. Int J Radiat Oncol Biol Phys 2000;48:289–302.
54. Drabik DM, Mackensie MA, Fallone GB. Quantifying appropriate PTV setup margins: analysis of patient setup fidelity and intrafraction motion using post-treatment megavoltage computed tomography scans. Int J Radiat Oncol Biol Phys 2007;68:1222–8.
55. Aubry J, Beaulieu L, Girouard L, Aubin S, Tremblay D, Laverdière J, et al. Measurements of intrafraction motion and interfraction and intrafraction rotation of prostate by three-dimensional analysis of daily portal imaging with radiopaque markers. Int J Radiat Oncol Biol Phys 2004;60:30–9.
56. Britton KR, Takai Y, Mitsuya M, Nemoto K, Ogawa Y, Yamada S. Evaluation of inter- and intrafraction organ motion during intensity modulated radiation therapy (IMRT) for localized prostate cancer measured by a newly developed on-board image-guided system. Radiat Med 2005;23:14–24.
57. Chen J, Lee J, Handrahan D, Sause W. Intensity-modualted radiotherapy using implanted fiducal markers with daily portal imaging: assessment of prostate organ motion. Int J Radiat Oncol Biol Phys 2007;68:912–9.
58. Cheung P, Sixel K, Morton G, Loblaw DA, Tirona R, Pang G, et al. Individualized planning target volumes for intrafraction motion during hypofractionated intensity-modulated radiotherapy boost for prostate cancer. Int J Oncol Biol Phys 2005;62:418–25.
59. Ghilezan MJ, Jaffray DA, Siewerdsen JH, Van Herk M, Shetty A, Sharpe MB, et al. Prostate gland motion assessed with cine-magnetic resonance imaging (cine-MRI). Int Radiat Oncol Biol Phys 2005;62:406–17.
60. Kitamura K, Shirato H, Seppenwoolde Y, Onimaru R, Oda M, Fujita K, et al. Three-dimensional intrafractional movement of prostate measured during real-time tumor-tracking radiotherapy in supine and prone treatment positions. Int J Radiat Oncol Biol Phys 2002;53:1117–23.
61. Kotte A, Hofman P, Langemdijk JJW, van Vulpen M, van der Heide UA. Intrafraction motion of the prostate during external-beam radiation therapy: analysis of 427 patients with implanted fiducial makers. Int J Radiat Oncol Biol Phys 2007;69:419–25.
62. Nederveen AJ, van der Heide UA, Dehnad H, van Moorselaar RJA, Hofman P, Lagendijk JJW. Measurements and clinical consequences of prostate motion during a radiotherapy fraction. Int J Radiat Oncol Biol Phys 2002;53:206–14.
63. Noel C, Roy M, Parikh PJ, Kupelian P, Mahadevan A, Weinstein G, et al. Are pre and post imaging sufficient to assess intrafraction prostate motion? [Abstract]. Int J Radiat Oncol Biol Phys 2007;69:S22–3.
64. Adamson JD, Wu Q, Yan D, Ghilezan M. Direct measurement of prostate intrafraction motion and residual setup error [Abstract]. Int J Radiat Oncol Biol Phys 2008;72:S549.
65. Litzenberg DW, Balter JM, Hadley SW, Sandler HM, Willoughby TR, Kupelian PA, et al. Influence of intrafraction motion on margins for prostate radiotherapy. Int J Radiat Oncol Biol Phys 2006;65:548–53.
66. Willoughby TR, Kupelian PA, Pouliot J, Shinohara K, Aubin M, Roach M, et al. Target localization and real-time tracking using the Calypso 4D localization system in patients with localized prostate cancer. Int J Radiat Oncol Biol Phys 2006;65:528–34.
67. Kupelian P, Willoughby T, Mahadevan A, Djemil T, Weinstein G, Jani S, et al. Multi-institutional clinical experience with the Calypso System in localization and continuous, real-time monitoring of the prostate gland during external radiotherapy. Int J Radiat Oncol Biol Phys 2007;67:1088–98.
68. Bortfeld T, van Herk M, Jiang SB. When should systematic patient positioning errors in radiotherapy be corrected? Phys Med Biol 2002;47:N297–302.
69. Stroom JC, de Boer HCJ, Huizenga H, Visser AG. Inclusion of geometrical uncertainties in radiotherapy treatment planning by means of coverage probability. J Radiat Oncol Biol Phys 1999;43:905–19.
70. Harsolia AR, Vargas CE, Kestin LL, Yan D, Brabbins DS, Lockman DM, et al. Predictors for chronic urinary toxicity following treatment of prostate cancer with 3-D conformal radiotherapy: dose-volume analysis of a phase II dose escalation study [abstract]. Int J Radiat Oncol Biol Phys 2004;60:S437–8.
71. Kupelian PA, Reddy CA, Carlson TP, Willoughby TR. Dose-volume relationship of late rectal bleeding after external beam radiotherapy for localized prostate cancer: absolute or relative rectal volume? Cancer J 2002;8:62–6.
72. Schaly B, Kempe JA, Bauman GS, Battista JJ, Van Dyk J. Tracking the dose distribution in radiation therapy by accounting for variable anatomy. Phys Med Biol. 2004;49:791–805.
73. Shah AP, Langen KM, Ruchala KJ, Cox A, Kupelian PA, Meeks SL. Patient dose from megavoltage computed tomography imaging. Int J Radiat Oncol Biol Phys 2008;70:1579–87.
74. Walter C, Boda-Heggemann J, Wertz H, Loeb I, Rahn A, Lohr F, et al. Phantom and in-vivo measurements of dose exposure by image-guided radiotherapy (IGRT): MV portal images vs. kV portal images vs. cone-beam CT. Radiother Oncol 2007;85:418–23.